Efficient stimulus-secretion coupling at ribbon synapses requires RIM-binding protein tethering of L-type Ca^{2+} channels

Fujun Luo[a,b,1], Xinran Liu[c], Thomas C. Südhof[a,b,2], and Claudio Acuna[a,b,1,2]

[a]Department of Molecular and Cellular Physiology, Stanford University School of Medicine, Stanford, CA 94305; [b]Howard Hughes Medical Institute, Stanford University School of Medicine, Stanford, CA 94305; and [c]Department of Cell Biology, Yale University School of Medicine, New Haven, CT 06510

Contributed by Thomas C. Südhof, August 4, 2017 (sent for review February 22, 2017; reviewed by Peter Jonas, Susanne McGovern, and Gerald W. Zamponi)

Fast neurotransmitter release from ribbon synapses via Ca^{2+}-triggered exocytosis requires tight coupling of L-type Ca^{2+} channels to release-ready synaptic vesicles at the presynaptic active zone, which is localized at the base of the ribbon. Here, we used genetic, electrophysiological, and ultrastructural analyses to probe the architecture of ribbon synapses by perturbing the function of RIM-binding proteins (RBPs) as central active-zone scaffolding molecules. We found that genetic deletion of RBP1 and RBP2 did not impair synapse ultrastructure of ribbon-type synapses formed between rod bipolar cells (RBCs) and amacrine type-2 (AII) cells in the mouse retina but dramatically reduced the density of presynaptic Ca^{2+} channels, decreased and desynchronized evoked neurotransmitter release, and rendered evoked and spontaneous neurotransmitter release sensitive to the slow Ca^{2+} buffer EGTA. These findings suggest that RBPs tether L-type Ca^{2+} channels to the active zones of ribbon synapses, thereby synchronizing vesicle exocytosis and promoting high-fidelity information transfer in retinal circuits.

active zone | synaptic transmission | calcium current | nanodomain | RIM-BP

At synapses, fast Ca^{2+}-triggered neurotransmitter release occurs at specialized regions of the nerve terminal called active zones. Presynaptic active zones are composed of several large and evolutionarily conserved multidomain protein families, including Rab3-interacting molecules (RIMs), RIM-binding proteins (RBPs), MUNC13, ELKS, Bassoon, and Piccolo (1–3). Active zones perform at least four essential functions: They tether synaptic vesicles at release sites, they prime vesicles for fusion, they recruit Ca^{2+} channels into close proximity to release sites, and they align pre- and postsynaptic elements of synapses, possibly by organizing transsynaptic signaling complexes (3).

Recruitment of Ca^{2+} channels adjacent to release sites is essential for rapid and precise synaptic transmission. The underlying molecular mechanisms, however, are incompletely understood. Systematic analyses of RIM-deficient neurons have revealed that RIMs play a critical role in determining Ca^{2+}-channel density and localization in conventional central synapses by two mechanisms (4, 5). First, RIMs' central PDZ domains directly and selectively interact with C-terminal PDZ-domain-binding motifs of N- and P/Q-type Ca^{2+} channels (but not of L-type Ca^{2+} channels) to recruit them to the presynaptic active zone (5). Second, RIM proteins also indirectly interact with Ca^{2+} channels via RBPs. Specifically, RIMs contain central proline-rich sequences that tightly interact with SH3 domains of RBPs, which in turn directly bind to all presynaptic Ca^{2+}-channel subtypes (see below).

RBPs are large multidomain proteins that are encoded by three genes in vertebrates: *RBP1*, *RBP2*, and *RBP3* (6–8). RBP1 and RBP2 proteins are mainly produced in the brain while RBP3 is primarily synthesized in nonneural tissues (6). All RBPs are composed of one central and two C-terminal SH3 domains separated by three fibronectin-like-3 (FN3) domains. RBPs interact, via their SH3 domains, not only with RIMs but also with cytoplasmic proline-rich sequences of L-, P/Q-, and N-type Ca^{2+} channels (5, 8–10). The role of RBPs in presynaptic Ca^{2+}-channel localization and function in conventional synapses has recently been addressed in flies and mice (11–13). In *Drosophila*, deletion of the single RBP gene reduced Ca^{2+}-channel abundance and Ca^{2+} influx, decreased the number of docked vesicles, disrupted the integrity of the active zone cytomatrix, and dramatically impaired Ca^{2+}-triggered neurotransmitter release (10, 13). In mice, however, deletion of RBP1 and RBP2 did not influence the properties or density of presynaptic P/Q- and N-type Ca^{2+} channels and produced only mild impairments in the extent of transmitter release in response to single spikes (11, 12). Remarkably, however, deletion of RBPs from murine synapses specifically interfered with the coupling of Ca^{2+} channels to synaptic vesicle exocytosis in response to spike trains and rendered action potential-mediated transmitter release highly unreliably under these conditions (11, 12).

Unlike RIMs, RBPs can bind not only P/Q- and N-type Ca^{2+} channels, but also L-type Ca^{2+} channels (9). In neurons, L-type Ca^{2+} channels mostly localize to dendritic compartments and are not required for neurotransmitter release. However, in ribbon-type synapses of the retina and inner ear, L-type Ca^{2+} channels are the source of Ca^{2+} influx for evoked neurotransmitter release. Ribbon synapses are specialized to support rapid and sustained transmitter release (refs. 14 and 15 and Fig. 1*A*, *Left*), and their eponymous synaptic ribbons are thought to provide a continuous supply of synaptic vesicles for release to support rapid and sustained release (16). In addition, L-type Ca^{2+} channels that mediate evoked release at ribbon synapses in-

Significance

This paper investigates the organization of the active zone at ribbon synapses in the retina, using deletions of the active zone protein RIM-binding protein (RBP) as a tool. The results demonstrate that, at these synapses, which, different from other synapses, use presynaptic L-type calcium channels for triggering vesicle exocytosis, RBPs mediate the recruitment of L-type calcium channels adjacent to release sites, thereby allowing efficient stimulus-secretion coupling. Thus, this paper presents a demonstration of how calcium channels are organized at the presynaptic active zone of ribbon synapses.

Author contributions: F.L., T.C.S., and C.A. designed research; F.L., X.L., and C.A. performed research; F.L. and C.A. contributed new reagents/analytic tools; F.L., T.C.S., and C.A. analyzed data; and F.L., T.C.S., and C.A. wrote the paper.

Reviewers: P.J., Institute of Science and Technology; S.M., University of Bonn; and G.W.Z., University of Calgary.

The authors declare no conflict of interest.

[1]F.L. and C.A. contributed equally to this work.

[2]To whom correspondence may be addressed. Email: tcs1@stanford.edu or claudioa@stanford.edu.

This article contains supporting information online at www.pnas.org/lookup/suppl/doi:10.1073/pnas.1702991114/-/DCSupplemental.

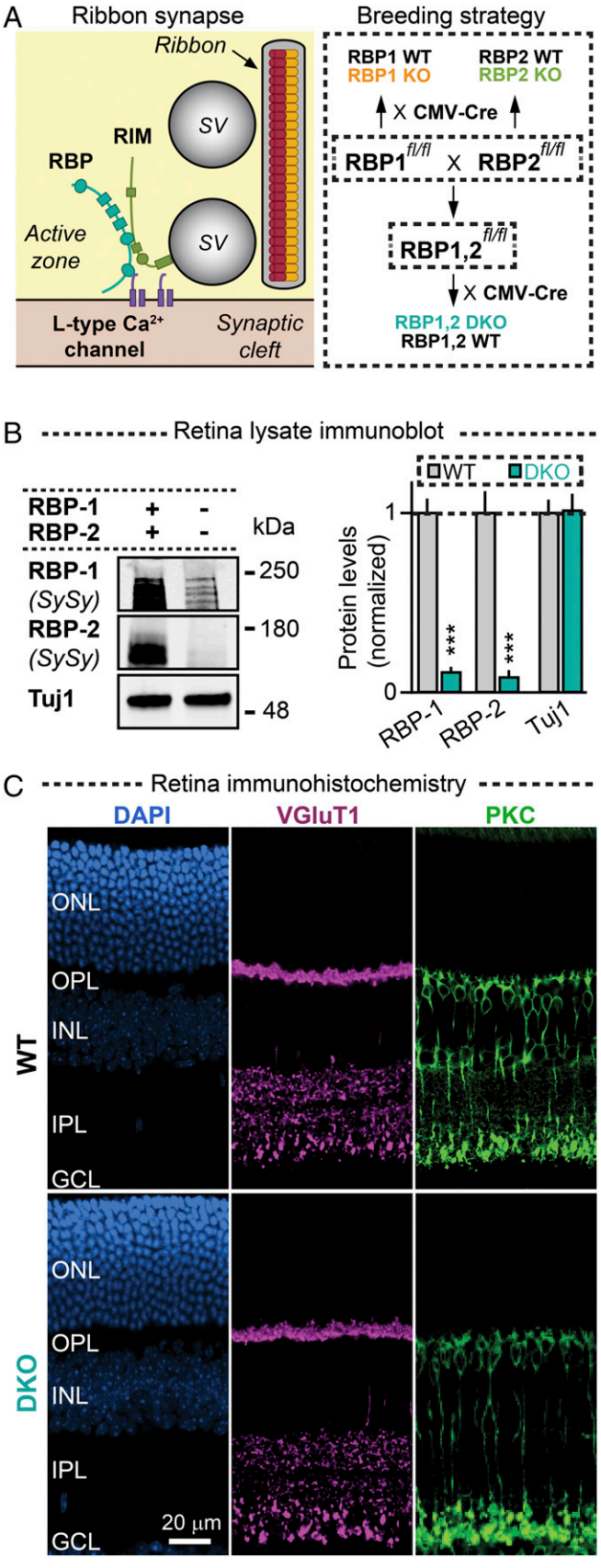

Fig. 1. Genetic deletion of RBPs does not alter the overall architecture of the retina. (*A*, *Left*) Schematic of a ribbon synapse highlighting RBP interactions with RIM and L-type Ca^{2+} channels. (*Right*) Diagram of the breeding strategy used to generate constitutive RBP1 KO, RBP2 KO, and RBP1,2 DKO mice and their respective littermate controls (based on RBP1,$2^{fl/fl}$ mice described in ref. 11). (*B*) Immunoblot analysis of RBPs in retina lysates from WT and RBP DKO mice (*Left*, representative blots; *Right*, summary graphs) (means ± SD, $n = 4$ WT and RBP DKO mice; statistical analyses by Student's *t* test; $***P < 0.001$; n.s., nonsignificant). The remaining RBP immunoblotting signal in DKO mice is likely due to nonspecific antibody cross-reactivity. (*C*) Immunofluorescence images of thin retina sections obtained from a WT (*Top*) and an RBP DKO (*Bottom*) mouse. Retina cryosections were stained with DAPI (blue) and antibodies against vGlut1 (purple) and PKCα (green). GCL, ganglion cell layer; INL, inner nuclear layer; IPL, inner plexiform layer; ONL, outer nuclear layer; OPL, outer plexiform layer.

activate more slowly than N- and P/Q-type Ca^{2+} channels at central synapses (15, 17), allowing ribbon synapses to support more prolonged Ca^{2+} influx upon presynaptic depolarization. Lastly, fast neurotransmitter release from ribbon synapses is known to rely on Ca^{2+} nanodomains, which requires tight coupling of Ca^{2+} channels to release-ready synaptic vesicles at the presynaptic active zone (14, 18). Despite the obvious significance of the clustering of presynaptic Ca^{2+} channels in ribbon synapses, however, relatively little is known about the molecular mechanisms of such clustering.

Here, we hypothesized that presynaptic RBPs recruit L-type Ca^{2+} channels to the active zone of ribbon synapses and mediate nanodomain coupling of L-type Ca^{2+} channels to release-ready vesicles. To test this hypothesis, we analyzed RBP-deficient mouse retinas using a combination of biochemistry, electrophysiology, and electron microscopy. Our results indicate that RBP1 and RBP2 determine the density and distribution of presynaptic L-type Ca^{2+} channels at ribbon synapses between rod bipolar and amacrine type-2 (AII) cells, thereby regulating the speed and synchrony of graded neurotransmitter release in retinal circuits.

Results

Deletion of RBPs Does Not Impact the Overall Architecture of the Retina. To test the role of RBPs in ribbon synapses, we crossed RBP1, RBP2, or RBP1,2 conditional knockout (KO) mice (RBP1$^{fl/fl}$, RBP2$^{fl/fl}$, and RBP1,2$^{fl/fl}$) (11) to a CMV-Cre mouse line that expressed cre-recombinase under control of the CMV minimal promoter in all tissues, including germ cells (19). In this manner, we generated constitutive RBP1 KO, RBP2 KO, or RBP1,2 double KO (DKO) mice (ref. 11 and Fig. 1 *A* and *B*).

We used light microscopy to study the structural organization of retinas obtained from WT and RBP-deficient DKO mice. Deletion of RBPs caused no major changes in the gross anatomy of the retina, including lamination of the two synaptic outer- and inner-plexiform layers, and did not alter the overall density of neurons of synapses (Fig. 1*C*). Thus, removal of RBPs does not cause major impairments in the architecture of the retina.

Deletion of RBPs Impairs Synaptic Transmission at Rod Bipolar Cells→AII Synapses. To study the role of RBPs in synaptic transmission at ribbon synapses, we performed high-resolution paired patch-clamp recordings from synaptically connected rod bipolar and AII amacrine cells (Fig. 2*A*). In these experiments, postsynaptic AII cells were maintained at a −70-mV holding potential, and presynaptic rod bipolar cells were sequentially depolarized from a holding potential of −70 mV to more positive potentials ranging from −50 mV to −20 mV; depolarizations were for 50 ms or 500 ms. These depolarization potentials are commonly observed in these synapses upon physiological activation with light (20, 21). As expected, in control retinas, presynaptic depolarizations above the L-type Ca^{2+}-channel activation threshold (~40 mV) induced robust Ca^{2+} currents and triggered pronounced fast synchronous neurotransmitter release,

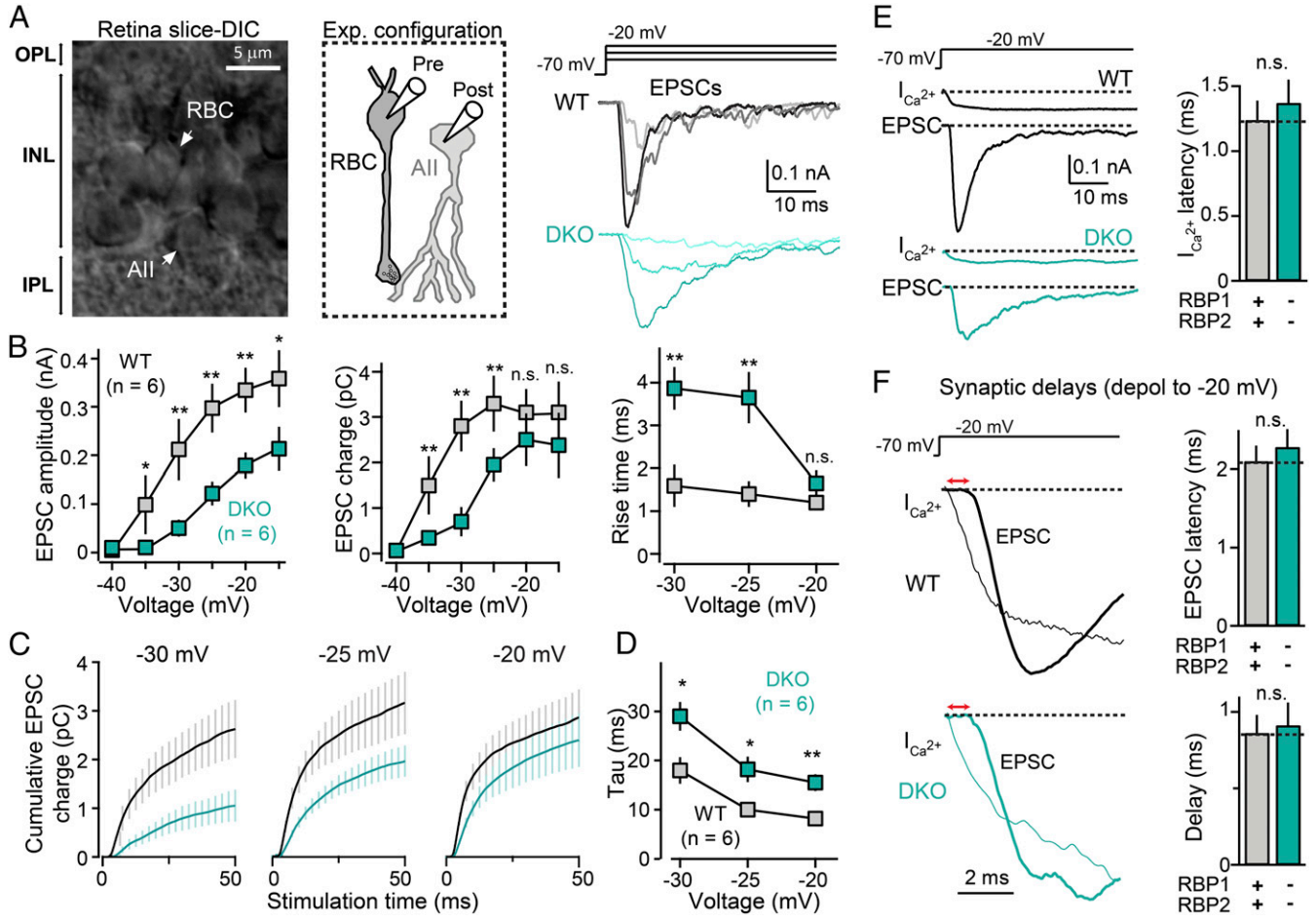

Fig. 2. Paired recordings reveal that deletion of RBPs severely affects synaptic transmission at ribbon synapses. (*A*) Experimental design for paired recordings from rod bipolar cell→AII amacrine cell synapses (*Left* and *Center*) and representative traces (*Right*). (*Left*) Infrared-differential interference contrast image of a retina slice used for patch-clamp recordings. (*Center*) Schematic of the recording configuration. (*Right Top*) Diagram of presynaptic depolarizations of rod bipolar cells; (*Right Bottom*) Representative EPSCs recorded from postsynaptic AII amacrine cells in WT and RBP DKO mice in response to the presynaptic rod bipolar cell depolarizations. Note that presynaptic patch-pipette solutions routinely contain 1 mM BAPTA to mimic intracellular Ca^{2+} buffers (31, 41). (*B*) Summary graphs of peak amplitudes (*Left*), total charge transfer (*Center*), and 20 to 80% rise times (*Right*) of EPSCs induced by presynaptic depolarization to −40 →−15 mV) in WT (gray) and RBP DKO (blue) synapses. (*C*) RBP deletion impairs the total amount and kinetics of synaptic transmission induced by prolonged presynaptic depolarizations. Plots of the mean cumulative EPSC charge transfer as a function of the time of presynaptic depolarization from −70 mV to −30 (*Left*), −70 mV to −25 (*Center*), or −70 mV to −20 mV (*Right*) in control (black) and mutant (blue) synapses ($n = 9$ for both). (*D*) Summary plot of the kinetics of the EPSC charge transfer induced by presynaptic depolarizations as in *C*. (*E* and *F*) Measurements of Ca^{2+}-current latency (*E*) and EPSC latency and synaptic delay (*F*). Presynaptic Ca^{2+} currents and postsynaptic EPSCs were simultaneously monitored using paired recordings from bipolar and AII amacrine cells from WT (black) and a RBP DKO (blue) synapse in these experiments. (*E*, *Left*) Representative dual recordings from rod bipolar cells and AII cells (*Bottom*). The protocol used to activate release from presynaptic bipolar cells is shown on *Top* and corresponds to depolarizations to −20 mV. (*E*, *Right*) Summary of Ca^{2+}-current latencies in six RBP control and six RBP DKO synapses. (*F*, *Left*) Overlapping recordings of presynaptic ICa^{2+} (thin line) and postsynaptic EPSC (thick line) in a WT (*Center*) and a DKO (*Bottom*) synapse. The red horizontal arrows represent synaptic delays. Traces have been normalized in the *y* axes to allow more precise measurements of synaptic delays. (*F*, *Right*) Summary graphs of EPSC latency and synaptic delays for six control and six DKO synapses. All summary graphs are mean ± SD. Statistical analyses were performed by either Student's *t* test (*D*–*F*) or by ANOVA followed by a Bonferroni post hoc test (*B* and *C*), comparing RBP DKO with WT (*$P < 0.05$, **$P < 0.01$; n.s., nonsignificant).

as measured via the peak amplitude of the corresponding excitatory postsynaptic currents (EPSCs) monitored in AII cells, as well as via the EPSC synaptic charge transfer (Fig. 2*A*). In contrast, deletion of RBPs strongly reduced presynaptic Ca^{2+} currents (see Fig. 4 for full analysis of this phenotype) and led to a pronounced reduction in neurotransmitter release (Fig. 2 *A*, *Right* and *B*, *Left* and *Center*), consistent with the notion that genetic ablation of RBPs decreases the initial release probability in these synapses.

We next analyzed in detail the kinetics of synaptic transmission in the same experiments. We first measured rise times of postsynaptic responses and found that the kinetics of EPSCs was impaired by deletion of RBPs, as indicated by the increased 20 to 80% rise times (Fig. 2*B*, *Right*). To more precisely estimate the effect of the RBP deletion on transmission, we integrated synaptic responses recorded from AII cells for presynaptic depolarizations to −30, −25, and −20 mV (Fig. 2 *C* and *D*). We found that deletion of RBPs not only reduced overall synaptic transmission (Fig. 2*C*) but also made transmission significantly slower (Fig. 2*D*), consistent with our direct measurements of the EPSC parameters described above. We then estimated the Ca^{2+}-current latency (Fig. 2*E*) (Δt between presynaptic depolarization and presynaptic Ca^{2+} current), EPSC latency (Fig. 2*F*, *Left*) (Δt between presynaptic depolarization and postsynaptic EPSC), and synaptic delay (Fig. 2*F*, *Right*) (difference between EPSC latency and Ca^{2+}-current latency). These measurements were performed

after depolarizing presynaptic bipolar cells to −20 mV. We failed to detect significant differences between control and RBP-deficient synapses in any of these parameters (Fig. 2 *E* and *F*). Together, our results thus indicate that RBPs control the extent and speed of evoked neurotransmitter release triggered by physiologically relevant patterns of presynaptic activation.

Deletion of RBPs Impairs the Kinetics of Emptying and Replenishing of the Readily Releasable Pool of Vesicles. A recent study in *Drosophila* neuromuscular junctions suggested that RBPs contribute to the replenishment of synaptic vesicles into the readily releasable pool (RRP) (10), but no similar activity was detected in mammalian central synapses (11). To determine whether RBP performs an RRP replenishment function in mammalian ribbon synapses, we examined the size and kinetics of the RRP. We depolarized presynaptic rod bipolar cells from −70 mV to −10 mV for 50 ms and recorded postsynaptic responses from AII cells in voltage clamp mode (Fig. 3*A*). This protocol is known to induce maximal Ca^{2+} influx into the presynaptic terminals of bipolar cells, thereby triggering release of the entire RRP (22). Interestingly, we did not observe significant differences in the size of the RRP in DKO synapses compared with controls. Instead, we found that both the rise time and decay time of postsynaptic responses were significantly slower in RBP-deficient synapses (Fig. 3 *B* and *C*). This phenotype suggests a desynchronization of vesicle fusion upon removal of RBPs, which resembles the phenotype we recently identified in conventional central synapses in mice (11).

We then measured the rate of RRP replenishment in control and RBP DKO synapses (Fig. 3 *D*–*F*). To measure replenishment

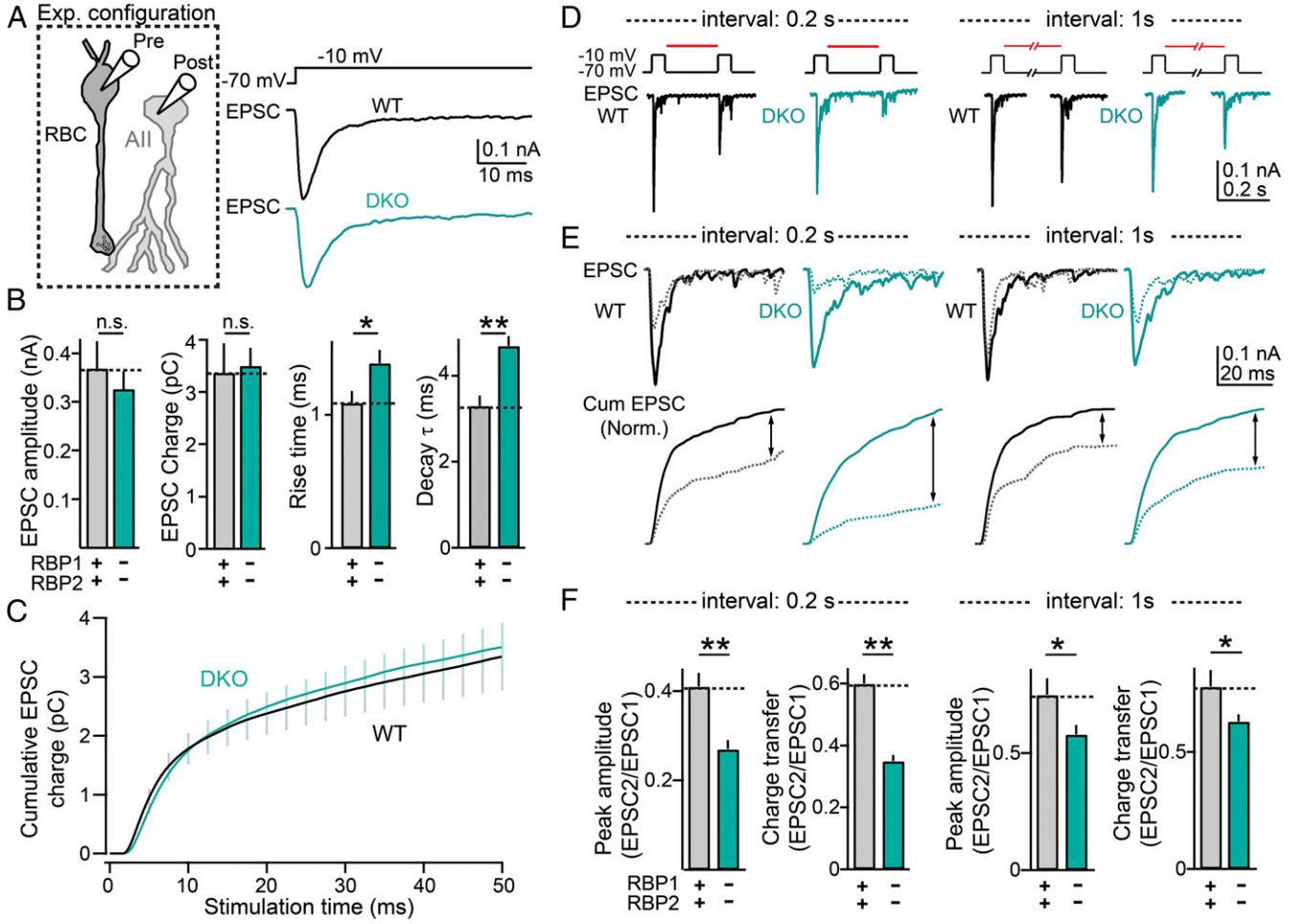

Fig. 3. Deletion of RBPs impairs the speed of both RRP emptying and RRP replenishment. (*A*, *Left*) Schematic of recording configuration. (*Right*) Representative postsynaptic recordings in an RBP WT (black) and an RBP DKO (blue) synapse. Transmitter release was triggered by presynaptic rod bipolar cell depolarization from −70 to −10 mV for 50 ms. All these experiments were performed in the presence of 1 mM BAPTA in the presynaptic pipette. (*B*) Summary graphs of RRP properties. RRP size and properties were estimated by recording EPSCs in AII cells after maximal activation of presynaptic bipolar cells, as indicated in *A*. From *Left* to *Right*, the following parameters are displayed: EPSC amplitude, EPSC charge transfer, EPSC 20 to 80% rise time, and EPSC decay time constant. Number of experiments: RBP WT, seven pairs; RBP DKO, seven pairs. (*C*) Time course of RRP emptying. Summary graph of integrated EPSC charge transfer as a function of time. EPSCs were triggered by maximal presynaptic depolarization as indicated in *A*. (*D*) Measurements of RRP recovery kinetics in RBP WT (*Left*) and RBP DKO synapses (*Right*). (*Top*) Presynaptic protocols used to deplete the RRP and to measure RRP recovery. Note that RRP recovery was measured at two time intervals: 0.2 and 1 s. (*Bottom*) EPSCs used to estimate RRP size and recovery. (*E*) RRP replenishment in ribbon synapses. (*Top*) Overlapping EPSCs showing RRP recovery dynamics for 0.2-s (*Left*) and 1-s (*Right*) intervals in representative RBP WT and DKO synapses. (*Bottom*) Normalized integrated responses as a function of time for the same experiment presented above. (*F*) Summary graphs of RRP recovery for 0.2-s and for 1-s time intervals. From *Left* to *Right*, the following parameters are displayed: EPSC amplitude recovery at 0.2-s intervals, EPSC charge recovery at 0.2-s intervals, EPSC amplitude recovery at 1-s intervals, and EPSC charge recovery at 1-s intervals. Number of experiments: RBP WT, five pairs; RBP DKO, five pairs. All summary graphs are mean ± SD. Statistical analyses were performed by either Student's *t* test (*B* and *F*) or by ANOVA followed by a Bonferroni post hoc test (*C*), comparing RBP DKO with RBP WT. (**P* < 0.05, and ***P* < 0.01; n.s., nonsignificant).

rates, we first depleted the RRP with a 50-ms depolarizing pulse to −10 mV, as above, and then applied a second test pulse (50-ms depolarization to −10 mV) at intervals of 0.2 s or 1 s (Fig. 3*D*, *Top*). We observed that the degree of RRP recovery was significantly reduced in RBP DKO synapses compared with control synapses for both interstimulus intervals (Fig. 3 *E* and *F*). Altogether, these results indicate that RBPs do not control the total number of primed synaptic vesicles but regulate the speed at which primed synaptic vesicles can be released from ribbon terminals upon prolonged Ca^{2+} influx. Moreover, as observed in *Drosophila* neuromuscular synapses (10), our results indicate that RBPs are important for RRP refilling at ribbon synapses.

Deletion of RBPs Reduces the Density of Presynaptic L-Type Ca^{2+} Channels. Our results above establish that RBPs strongly impair Ca^{2+}-triggered release from ribbon synapses. Because RBPs directly interact with L-type Ca^{2+} channels that mediate release from these synapses (5, 9), we asked if removal of RBPs might disrupt Ca^{2+}-channel density and/or function. We first studied how deletion of RBPs affects the level of presynaptic L-type Ca^{2+} channels by immunohistochemistry. We fixed retinas from control and RBP-deficient DKO mice with 4% paraformaldehyde, cut them into 50-μm-thick sections, and immunostained them with antibodies against CaV1.3. We observed a specific and significant reduction in the fluorescent signals for CaV1.3-containing Ca^{2+} channels in rod bipolar cell boutons, with no other obvious changes in bouton size or morphology (Fig. 4 *A*–*C*).

We then directly measured presynaptic Ca^{2+}-channel density using patch-clamp electrophysiology. We prepared relatively thin (200-μm) retina slices from control and RBP DKO mice and patch-clamped presynaptic rod bipolar cells (Fig. 4*D*, *Left*). To determine if RBP deletion impacts presynaptic L-type Ca^{2+} channels, we sequentially depolarized bipolar cells for 50 ms from a holding membrane potential of −70 mV to more depolarized potentials, ranging from −40 mV to −10 mV with 5-mV increments, and measured the corresponding Ca^{2+} currents using somatic whole-cell voltage-clamp recordings (Fig. 4*D*, *Right*). Rod bipolar cells lack expression of Ca^{2+} channels in their somato-dendritic compartments, and thus Ca^{2+} currents recorded under these conditions arise exclusively from release-relevant channels localized at the nerve terminal (23). Remarkably, we found that removal of RBPs significantly reduced (~50%) the peak amplitude and total charge of Ca^{2+} currents (Fig. 4 *D*, *Right* and *E*), without changing their kinetics and activation curve. The remaining Ca^{2+} currents in RBP DKO (~50%) were completely blocked by nimodipine (10 μM).

We further studied if RBP1 and RBP2 independently or redundantly recruit Ca^{2+} channels at the active zone, comparing Ca^{2+} currents in rod bipolar cells of control mice or mice lacking only either RBP1 or RBP2. As shown in Fig. 4 *F*–*H*, deletion of

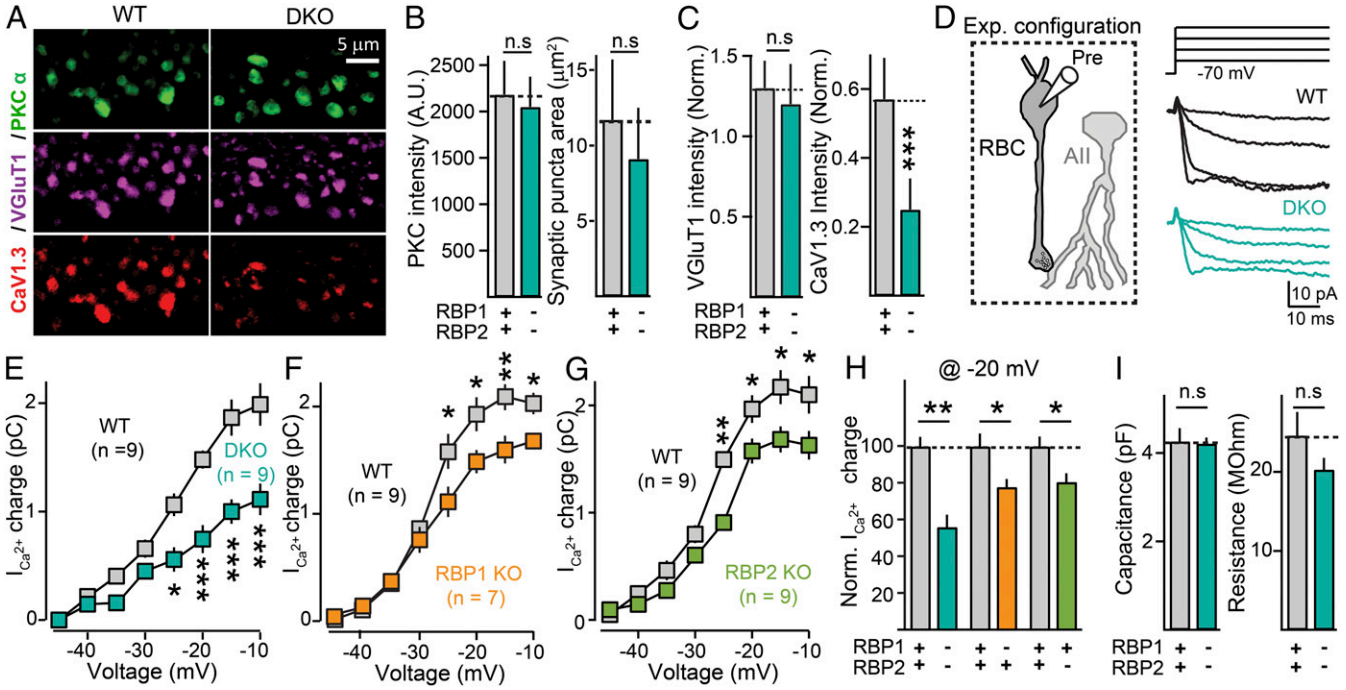

Fig. 4. Deletion of RBPs reduces Ca^{2+} currents in presynaptic rod bipolar cells forming ribbon synapses on postsynaptic AII amacrine cells. (*A*) Selective loss of presynaptic L-type Ca^{2+} channels from ribbon synapses formed by rod bipolar cells. Representative confocal images of RBP WT (*Left*) and RBP DKO (*Right*) retina sections stained for PKCα (green, to identify rod bipolar neurons), VGlut1 (purple, to identify presynaptic terminals), and the L-type Ca^{2+}-channel CaV1.3 (red). (*B*) Summary graphs of the intensity of PKCα fluorescent signals in WT(gray) and DKO (blue) rod bipolar cell terminals (*Left*), and terminal size (area, *Right*) defined by PKC staining. Number of experiments (images/mice): RBP WT, 79/3; RBP DKO, 70/3. (*C*) Relative vGluT1 (*Left*) and CaV1.3 (*Right*) staining intensity normalized by PKCα signals. Number of experiments (images/mice): RBP WT, 79/3; RBP DKO, 70/3. (*D*) Experimental configuration for Ca^{2+}-current recordings (*Left*) and representative experiment (*Right Top*) schematic of depolarization protocol; (*Right Bottom*) Sample traces for an RBP control (black) and an RBP DKO (blue) bipolar cell. (*E*) Deletion of RBP1,2 severely impairs presynaptic Ca^{2+}-current density. Summary plot of the Ca^{2+}-current charge transfer over 50 ms as a function of the membrane voltage in RBP1,2 DKO (blue) rod bipolar cells and corresponding littermate controls (gray). (*F* and *G*) Incremental contribution of RBP1 (*F*) and RBP2 (*G*) to the presynaptic Ca^{2+}-channel density of ribbon synapses. Same as *E*, but for littermate control (*F* and *G*, gray) and RBP1 KO (*F*, orange) or RBP2 KO (*G*, green) mice. (*H*) Summary graphs of the Ca^{2+}-current charge transfer induced by a 50-ms depolarization to −20 mV in RBP1,2 DKO, RBP1 KO, or RBP2 KO mice, normalized to the controls analyzed in the same experiments. Number of experiments as in *E*–*G*. (*I*) Summary graphs of whole-cell capacitance (*Left*) and input resistance (*Right*) in the same rod bipolar cells used to measure whole-cell presynaptic Ca^{2+} currents. Number of experiments as in *E*. All summary graphs are mean ± SD. Statistical analyses were performed by either Student's *t* test (*B*, *C*, *H*, and *I*) or by ANOVA followed by a Bonferroni post hoc test (*E*–*G*), comparing RBP DKO with RBP WT (*$P < 0.05$, **$P < 0.01$, and ***$P < 0.001$; n.s., nonsignificant).

either RBP1 or RBP2 reduced Ca^{2+} currents by ~20 to 30% compared with control littermates, without changing the capacitance or membrane resistance of rod bipolar cells (Fig. 4*I*), suggesting that RBP1 and RBP2 are both required for presynaptic Ca^{2+}-channel clustering and incrementally determine active zone L-type Ca^{2+}-channel density in ribbon synapses. Taken together, these results indicate that, in contrast to conventional mammalian synapses (11, 12), RBPs at ribbon synapse determine the density of active zone L-type Ca^{2+} channels, which is similar to the role of RBP in invertebrate synapses (10, 13).

Deletion of RBPs Alters the Biochemical Composition but Not the Ultrastructure of Retinal Ribbon Synapses. The strong reduction in presynaptic Ca^{2+}-channel density in RBP-deficient presynaptic ribbon terminals prompted us to examine whether RBP deletion may also impair the overall biochemical composition of retinal synapses. To address this question, we compared the levels of different Ca^{2+}-channel subtypes, active zone proteins, and proteins involved in late steps of synaptic vesicle exocytosis in extracts of retinas obtained from control or RBP DKO mice (Fig. 5). We first focused on the Cav1.2, Cav1.3, or Cav1.4 α-subunits of Ca^{2+} channels. Interestingly, we found that deletion of RBPs resulted in a significant increase in total expression of all α-subunits whereas the levels of β1–4 subunits remained unchanged (Fig. 5*A*). In contrast, the auxiliary $\alpha_2\sigma$ subunits, which are thought to play a role in targeting functional Ca^{2+} channels to the synapse (24), were significantly reduced (Fig. 5*A*).

We then measured the level of several active zone proteins (Fig. 5*B*). We found that Ribeye, Munc13, Liprinα3, Mint1, and CASK were not significantly changed. Surprisingly, RIMs and ELSKs, two important active zone molecules known to promote presynaptic clustering of Ca^{2+} channels (5, 25), were significantly increased in RBP-deficient retinas compared with WT controls. Finally, we assessed the levels of the SNARE proteins Syntaxin-1, SNAP-25, and Synaptobrevin-2, and of the fast Ca^{2+} sensor Synaptotagmin-1, but found no significant differences between control and RBP DKO retinas (Fig. 5*B*). Together, these results indicate that deletion of RBPs leads to selective but significant changes in retinal protein levels, which may directly or indirectly impair synaptic function.

To determine if changes in protein composition of nerve terminals upon removal of RBPs might result in morphological alterations of synapses, we studied in detail the fine structure of retina ribbon synapses using transmission electron microscopy (TEM) (Fig. 6). We found that the overall ultrastructure of ribbon synapses appeared normal in RBP DKO mice, compared with control littermates (Fig. 6*A*). We quantitatively measured several parameters, including synaptic ribbon length and area, number of docked vesicles, and number of vesicles in close association to the synaptic ribbons. However, we did not detect any significant differences between control and RBP DKO groups (Fig. 6*B*). Viewed together, these findings establish that deletion of RBPs does not change the fine structure of ribbon-type synapses in mice.

RBPs Couple Ca^{2+} Channels to Synaptic Vesicle Exocytosis at Bipolar Cells→AII Synapses. Our results thus far indicate that ablation of RBPs decreases and desynchronizes Ca^{2+}-triggered release (Fig. 2), impairs the kinetics of RRP emptying and replenishment (Fig. 3), and reduces presynaptic Ca^{2+}-channel density in retina ribbon synapses (Fig. 4). These phenotypes can potentially be accounted for by increases in the physical distance between Ca^{2+} channels and primed synaptic vesicles at the presynaptic active zone in RBP-deficient synapses. To directly test this possibility, we loaded rod bipolar cell terminals with high concentrations (10 mM) of the slow Ca^{2+} chelator EGTA via the patch pipette, depolarized nerve terminals from −70 to 10 mV for 50 ms, and recorded the resulting evoked EPSCs in AII amacrine cells in the absence (Fig. 7 *A–C*) or presence (Fig. 7 *D–F*) of 1 mM BAPTA. The Ca^{2+} chelator EGTA, because of its intrinsically slow Ca^{2+}-binding/unbinding rate, can selectively and efficiently suppress transmitter release mediated by Ca^{2+} channels loosely coupled to Ca^{2+} sensors attached to synaptic vesicles (26–30). Thus, changes in coupling distance between the Ca^{2+} channel and synaptic vesicles can be detected as changes in the relative EPSC sensitivity to defined presynaptic EGTA concentrations.

We observed that high concentrations of EGTA (10 mM) did not change the magnitude of fast/synchronous transmitter release in WT rod bipolar cells→AII synapses, regardless of the presence of 1 mM BAPTA in presynaptic terminals (Fig. 7), indicating that fast/synchronous release in this synapse involves nanodomain coupling of Ca^{2+} channels to synaptic vesicle exocytosis ($P > 0.05$ for direct comparison of EPSC amplitude without and with EGTA) (Figs. 3 *A* and *B* and 7 *D–F*) (22, 31). In striking contrast, in RBP-deficient synapses, 10 mM EGTA reduced fast/synchronous EPSC peak amplitude by ~50%; again, this change was observed in the presence or absence of 1 mM

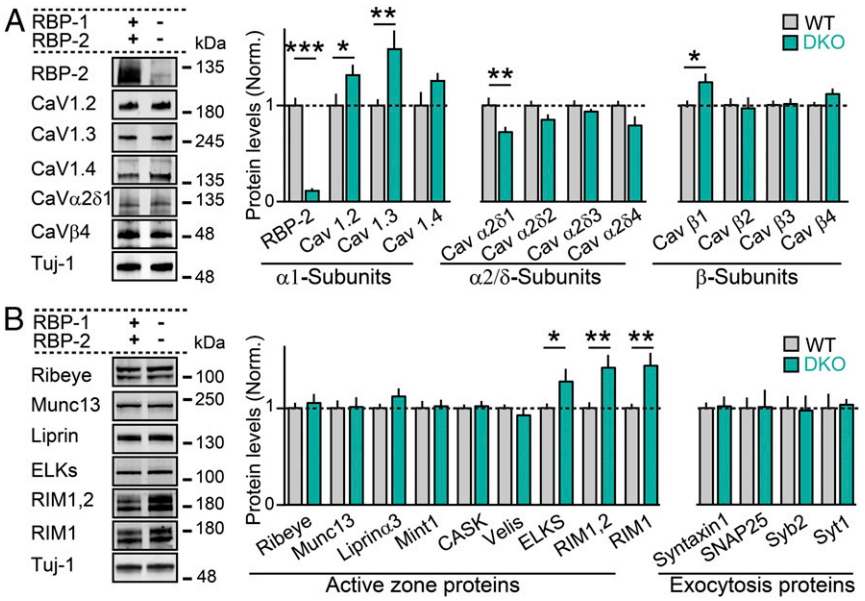

Fig. 5. Retina protein levels upon removal of RBPs. (*A*) Quantitative Western blot analysis of primary and auxiliary L-type Ca^{2+}-channel subunits in the mouse retina. (*Left*) Images of representative blots. (*Right*) Summary graphs for six RBP WT and seven RBP DKO experiments. (*B*) Same as in *A*, but for active zone and proteins involved in vesicle exocytosis. Number of experiments: six for WT retinas; seven for DKO retinas. All summary graphs are means ± SD. Statistical analyses were performed by Student's *t* test comparing RBP DKO with RBP WT (*$P < 0.05$, **$P < 0.01$, and ***$P < 0.001$; n.s., nonsignificant).

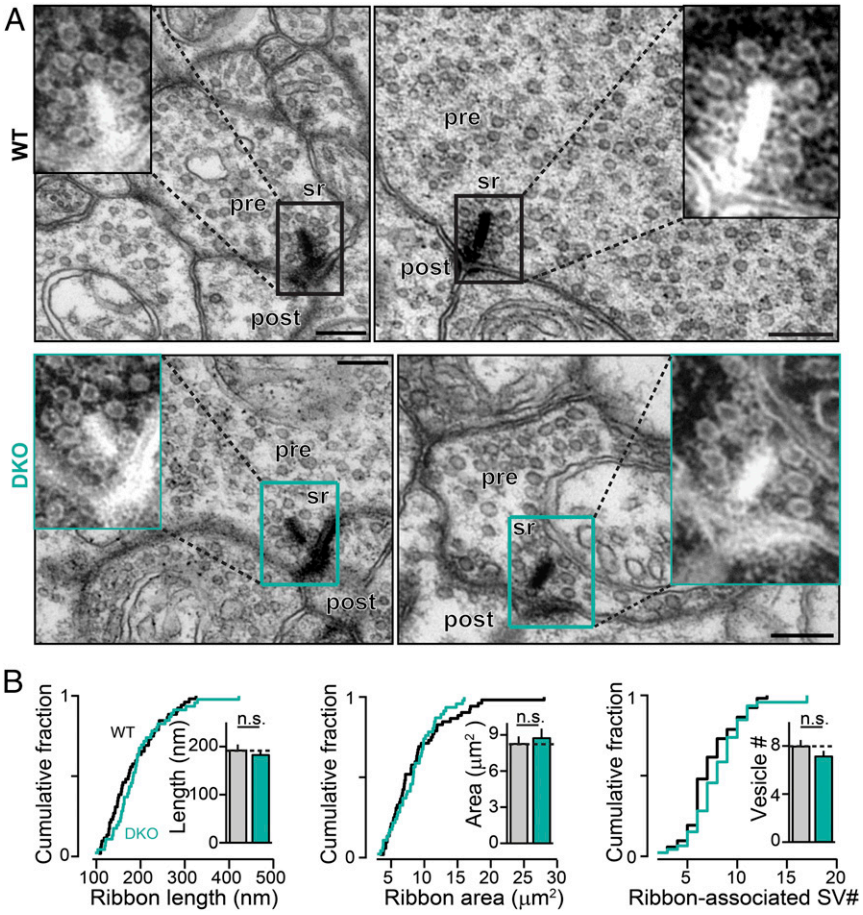

Fig. 6. Deletion of RBPs does not alter the ultrastructure of ribbon synapses. (*A*) High-resolution transmission electron microscopy images of retinal ribbon synapses in WT (*Top*) and RBP DKO (*Bottom*) retinas. (*Insets*) Enlarged images of the synaptic ribbons for each micrograph, with inverted contrast for better visualization of synaptic ribbons and associated vesicles. (Scale bar: 200 nm.) Post, postsynaptic; pre, presynaptic; sr, synaptic ribbon. (*B*) Cumulative distribution plots and bar graphs of the ribbon length (*Left*), ribbon area (*Center*), and total number of ribbon-associated vesicles (*Right*) in WT and RBP DKO retinas. n (synapses/mice) = 72/3 for WT; 97/3 for DKO sample. Summary graphs are means ± SD; statistical analyses were performed by the Kolmogorov–Smirnov (K-S) test (cumulative distributions) or Student's *t* test (bar graphs; n.s., nonsignificant).

presynaptic BAPTA (Fig. 7) (for direct comparison of EGTA effects on EPSC amplitude in RBP DKO synapses, see Figs. 3 *A* and *B* and 7 *D–F*) ($P < 0.05$). Moreover, EPSC rise times and decay times were significantly increased by EGTA in RBP-deficient ribbon synapses, but the total synaptic charge transfer was not greatly changed (Fig. 7 *B* and *E*). These results suggest that RBPs control the physical distance between L-type Ca^{2+} channels and primed synaptic vesicles that mediate fast transmitter release from ribbon synapses.

To further test this conclusion, we examined whether removal of RBPs also impairs coupling of Ca^{2+} channels to spontaneous synaptic vesicle exocytosis (Fig. 8). For this purpose, we measured the rate and properties of quantal miniature EPSCs (mEPSCs) in control and RBP-deficient AII cells in the absence and presence of EGTA (Fig. 8*A*). Ablation of RBPs did not significantly change the frequency, amplitude, or kinetic properties of AII mEPSCs (Fig. 8 *A*, *B*, and *D*). Moreover, incubation of the slices in 0.2 mM EGTA acetoxymethyl ester (EGTA-AM) for 45 min did not change the frequency, amplitude, or kinetic properties of mEPSCs in control slices (Fig. 8*E*). In RBP-DKO synapses, however, EGTA-AM treatment produced an almost complete ablation of mESPCs, with a reduction in mEPSC frequency of ~90% but no major changes in mEPSC amplitude or kinetic properties (Fig. 8*E*). Since mEPSCs are thought to be triggered at least in part by stochastic Ca^{2+}-channel opening (32), this result supports the notion that RBPs couple synaptic vesicles to Ca^{2+} channels.

Finally, we tested the effect of EGTA-AM on mEPSC frequency in RBP-deficient ribbon synapses via EGTA-AM "wash-in" experiments. We applied 0.2 μM EGTA-AM onto retina slices by perfusion and measured the effect of the EGTA-AM on mEPSC frequency in individual cells before and after EGTA-AM addition. Under these conditions, we found that EGTA-AM reduced mEPSC frequency by 62.7 ± 18.5% ($n = 4$, $P < 0.05$, estimated at 30 min after starting the perfusion of EGTA-AM). Again, these results are consistent with the notion that mEPSCs induced by stochastic opening of L-type Ca^{2+} channels are coupled to synaptic vesicles via RBPs in ribbon synapses.

Discussion

In the present study, we used a combination of morphological, biochemical, and electrophysiological analyses to assess the function of RBPs in ribbon synapses that are formed by rod bipolar cells on AII amacrine cells in the mouse retina. We found that, in these synapses, RBPs control the localization of presynaptic L-type Ca^{2+} channels at the active zone and determined the physical distance between these channels and release-ready synaptic vesicles for spontaneous and evoked transmitter release. We propose that, by tethering L-type Ca^{2+} channels to the active zone of ribbon synapses, RBPs promote efficient stimulus-secretion coupling and high-fidelity visual information transfer across retinal circuits.

We systematically dissected the functions of RBPs in the retinal ribbon synapses by constitutively deleting RBP1 and RBP2, the two major RBP isoforms expressed in neuronal tissues. In a series of detailed morphological studies using light and electron microscopy (Figs. 1 and 6), we showed that deletion of RBPs did not alter the overall organization of the retina or the ultrastructure of bipolar cell→AII amacrine cell ribbon synapses. These results differ from those reported in *Drosophila*, in which null mutations of RBP led to dramatic changes in the fine structure of neuromuscular synapses (13), but agree with analyses

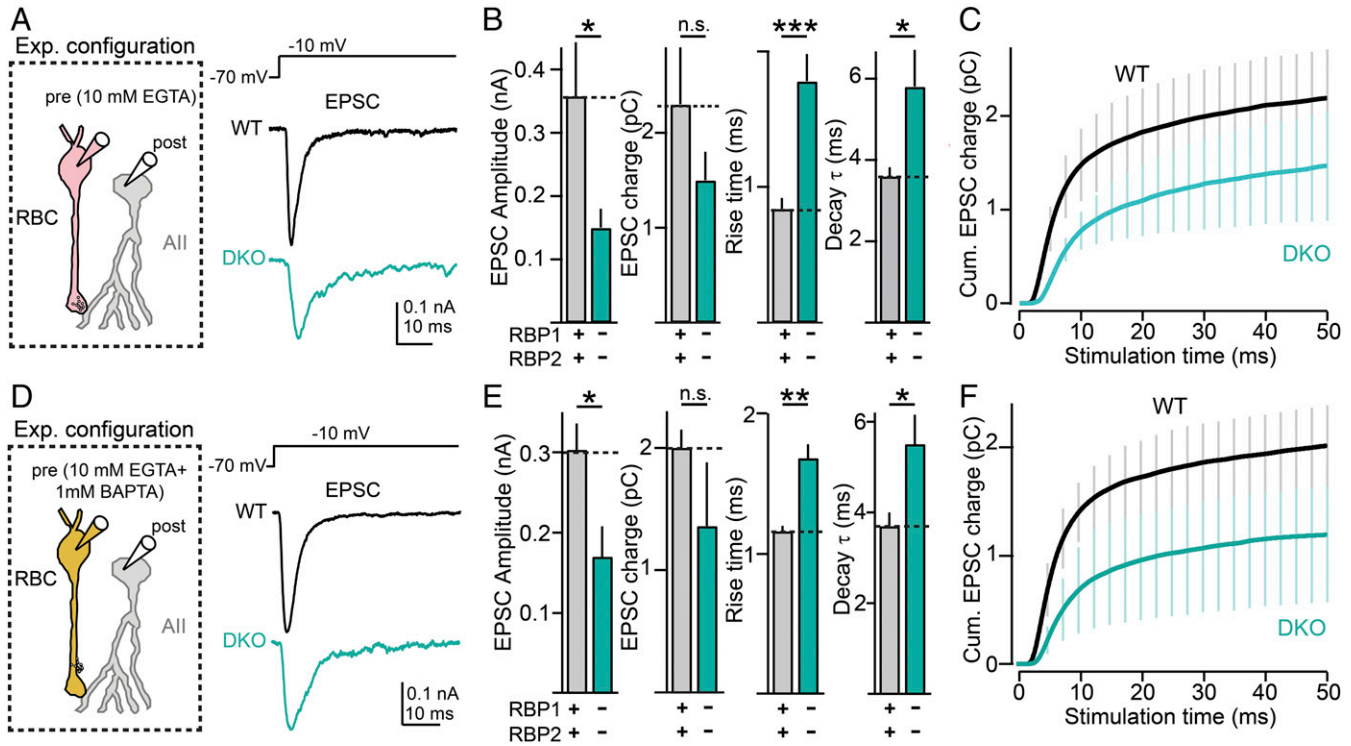

Fig. 7. Deletion of RBPs impairs tight coupling of Ca^{2+} channels to synaptic vesicle exocytosis. (*A–C*) Impact of presynaptic 10 mM EGTA on evoked transmission at rod bipolar cell→AII amacrine cell synapses. (*A*, *Left*) Schematic of recording configuration. (*Right*) Representative postsynaptic recordings in an RBP WT (black, *Center*) and an RBP DKO (blue, *Bottom*) synapse. Transmitter release was triggered by depolarizing presynaptic rod bipolar cells from −70 to −10 mV for 50 ms (black, *Top*). (*B*) Impact of 10 mM EGTA on evoked synaptic transmission at rod bipolar cells→AII synapses, triggered as in *A*. Summary plots of multiple evoked EPSC parameters in RBP WT (gray) and RBP DKO (blue) are shown. From *Left* to *Right*, the following parameters are displayed: EPSC amplitude, EPSC charge transfer, EPSC 20 to 80% rise time, and EPSC decay time constant. Number of experiments: RBP WT, six pairs; RBP DKO, six pairs. (*C*) Time course of evoked EPSC in the presence of 10 mM EGTA in WT (black) and mutant (blue) synapses. EPSCs were triggered by maximal presynaptic depolarization as indicated in *A*. (*D–F*) Same as in *A–C* but in the presence of additional 1 mM BAPTA in presynaptic terminals. Number of experiments: RBP WT, six pairs; RBP DKO, five pairs. All summary graphs are means ± SD. Statistical analyses were performed by either Student's *t* test (*B* and *E*) or by ANOVA followed by a Bonferroni post hoc test (*C* and *F*), comparing RBP DKO with RBP WT (*$P < 0.05$, **$P < 0.01$, and ***$P < 0.001$; n.s., nonsignificant).

of RBP mutants in conventional central murine synapses that revealed no major morphological abnormalities in synapse ultrastructure (11, 12, 33). Thus, in mice, RBPs are likely not essential for the formation and/or maintenance of active zones as such.

Using high-resolution patch-clamp recordings from rod bipolar cells, we directly recorded presynaptic Ca^{2+} currents. We found that deletion of RBPs resulted in a 50% reduction in Ca^{2+}-current density without changing Ca^{2+}-current activation and deactivation kinetics (Fig. 4). Both RBP1 and RBP2 contributed to the Ca^{2+}-channel density in an additive manner because separate deletions of either RBP isoform produced a 20 to 30% reduction in Ca^{2+} currents. Moreover, immunostaining of presynaptic bipolar cell terminals for Ca^{2+} channels showed that L-type Ca^{2+}-channel levels were reduced in RBP mutants, indicating that RBPs are required for recruiting Ca^{2+} channels to the release sites. Interestingly, measurements of whole-retina Ca^{2+}-channel levels by immunoblotting revealed an upregulation of all major subtypes of pore-forming subunits of L-type Ca^{2+} channels, suggesting a compensatory increase in Ca^{2+}-channel proteins (Fig. 5). The observation that L-type Ca^{2+}-channel expression is increased in RBP-deficient retinas but that the presynaptic Ca^{2+}-current density and Ca^{2+}-channel levels are decreased suggests that the additional Ca^{2+}-channel protein may be retained in intracellular compartments in the absence of targeting slots that are normally provided by RBPs.

Paired recordings from rod bipolar cells and AII amacrine cells revealed that removal of RBPs led to a dramatic reduction in the amount and speed of release triggered by presynaptic depolarization (Fig. 2). This is likely due to the fact that the remaining Ca^{2+} channels at active zones in the absence of RBPs (near 50%) are physically uncoupled from primed synaptic vesicles because evoked release in RBP DKO synapses was highly sensitive to the slow Ca^{2+}-buffer EGTA (Fig. 7). Thus, RBPs appear to recruit L-type Ca^{2+} channels to ribbon synapse active zones and to place them in close proximity to the sites of exocytosis to enable tight "nanodomain" coupling of Ca^{2+} influx to Ca^{2+}-triggered neurotransmitter release. It should be noted, however, that it is not clear whether the role of RBPs in coupling Ca^{2+} channels to release-ready vesicles as observed in retinal biopolar cell→AII cell synapses can be generalized to other ribbon synapses. For instance, in the hippocampus and cerebral cortex, the "tightness" of Ca^{2+}-channel coupling to release-ready vesicles seems to be target- and cell type-specific (34, 35). Although different types of ribbon synapses appear to be more similar to each other than the different types of conventional synapses examined in studies on nanodomain coupling, it will be interesting to determine whether ribbon synapses other than bipolar cell→AII amacrine cell synapses are also controlled by RBPs.

In addition to their role in Ca^{2+}-channel localization, we found that RBPs in ribbon synapses contribute to replenishment of synaptic vesicles into the RRP. This finding, different from the lack of ultrastructural changes in RBP-deficient synapses, is consistent with studies in *Drosophila* (10). Specifically, we observed that deletion of RBPs decelerated the kinetics of RRP

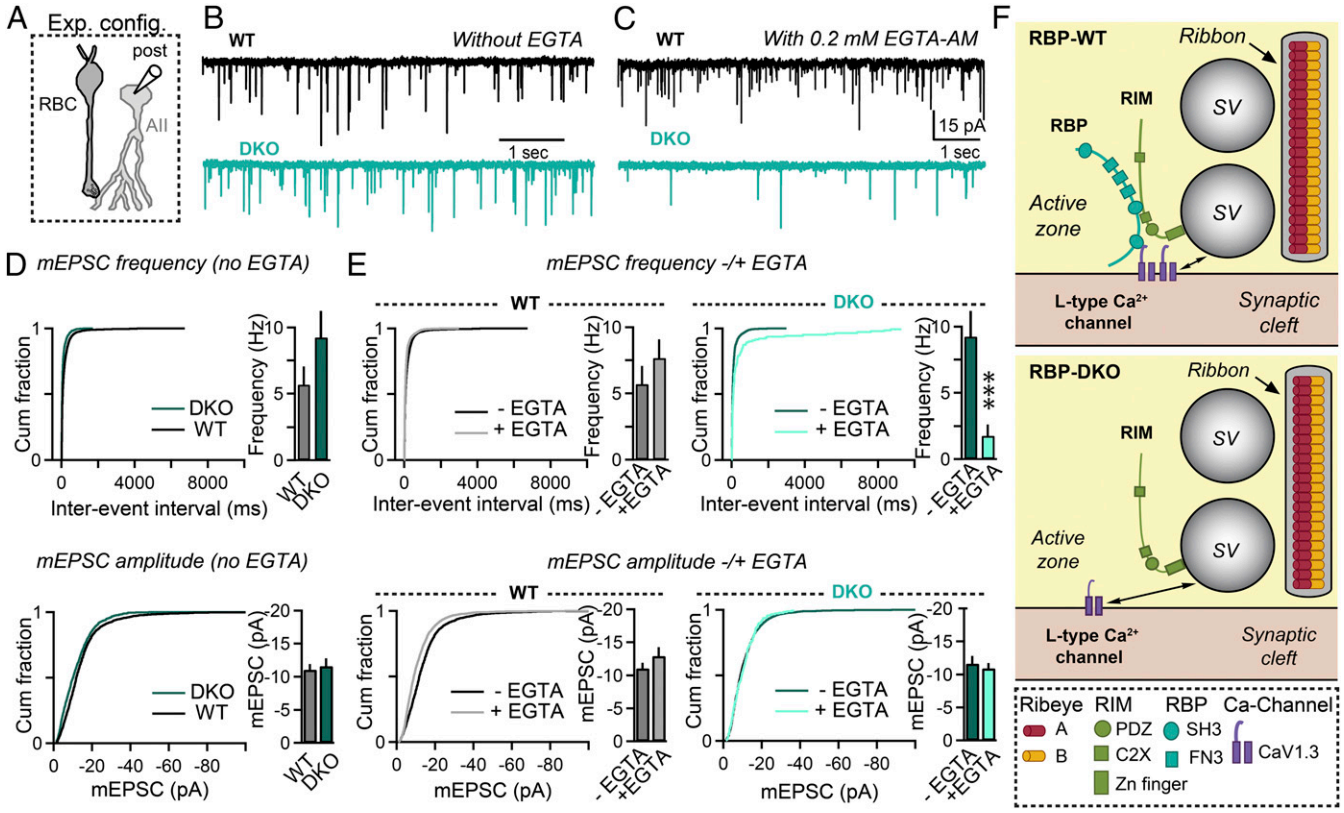

Fig. 8. Deletion of RBPs alters the sensitivity of quantal release to the slow Ca^{2+} buffer EGTA at rod bipolar cell to AII amacrine cell synapses. (*A*) Schematic of the recording configuration. (*B* and *C*) Spontaneous mEPSCs recorded from AII amacrine cells in RBP WT (black) and RBP mutant (blue) retinas, without external EGTA-AM (*B*) or in the presence of 0.2 mM EGTA-AM in the external solution (*C*). All these experiments were performed in the presence of GABAA receptor blockers. (*D*) Summary graphs of mEPSC frequency (*Top*) and mEPSC amplitude (*Bottom*) in RBP control (black) and RBP mutant (blue) retinas without EGTA-AM in the external solution. Number of experiments: RBP WT, 10 cells; RBP DKO, nine cells. (*E*) Summary graphs of mEPSC frequency (*Top*) and mEPSC amplitude (*Bottom*) in RBP control and RBP mutant retinas before (dark traces) and after (light traces) incubation with 0.2 mM EGTA-AM for 45 min. Number of experiments: RBP WT, nine cells; RBP DKO, nine cells. (*F*) Model summarizing the effects of deleting RBPs on the structure and function of retina ribbon synapses. All summary graphs are mean ± SD. Statistical analyses for data displayed in bar graphs were performed by Student's *t* test, comparing RBP DKO with RBP WT, whereas statistical analyses for data displayed in cumulative distribution plots were performed by K-S test (***$P < 0.001$; n.s., nonsignificant).

emptying and replenishing. While the effect of the RBP deletion on RRP emptying can be readily explained by the impairments in the coupling of the Ca^{2+} channel to synaptic vesicle exocytosis, as discussed above, its effect on RRP replenishment suggests a specific role for RBPs in vesicle priming, as observed earlier (10, 33). The exact mechanism underlying RBP control of vesicle replenishment remains uncertain but is most likely related to the recruitment of Munc13, the most important priming factor at synapses, to release sites by RIMs, which in turn are bound to RBPs (3).

Deletion of RBPs did not have a major impact on spontaneous quantal minirelease in ribbon synapses. This was somewhat surprising because mEPSCs in AII amacrine cells are thought to depend, at least in part, on stochastic openings of presynaptic Ca^{2+} channels and extracellular Ca^{2+} influx (32). Thus, considering the strong reduction in the density of presynaptic Ca^{2+} channels, a reduction in the frequency of mEPSCs in RBP mutants would have been expected. The most parsimonious explanation for the lack of an effect of the RBP deletion on mEPSCs is that evoked and spontaneous transmitter release are mechanistically different and may depend on different pools of synaptic vesicles (36–38). Consistent with this hypothesis, previous studies—including our own—have established that, in conventional excitatory synapses, RBPs selectively control evoked but not spontaneous neurotransmitter release (11, 12, 33). Lastly, although the RBP deletion did not affect spontaneous minirelease under physiological conditions, it dramatically increased the EGTA sensitivity of spontaneous release (Fig. 8). This finding is consistent with the conclusion that the RBP deletion increases the distance between Ca^{2+} channels and the sites for spontaneous vesicle exocytosis, without controlling the total number of these sites at the active zone, but does not quite explain why the resting mEPSC frequency is unchanged, a question that will need further experimental studies.

Mechanistically, RBPs likely cooperate with RIMs to localize Ca^{2+} channels to the active zone of ribbon synapses (39) and to prime and tether vesicles at release sites, similar to their cooperative function at conventional central synapses (33). What is different between conventional central synapses and ribbon synapses, however, is that the latter use L-type Ca^{2+} channels for release whereas the former use N- and/or P/Q-type Ca^{2+} channels (40). This is important because RBPs directly bind to proline-rich sequences via their three SH3-type domains in all of these Ca^{2+} channels whereas RIMs bind only to N- and P/Q-type Ca^{2+} channels (5, 9). The observation that the RBP deletion leads to a depletion of presynaptic Ca^{2+} channels in rod bipolar cells forming ribbon synapses, but not in the standard calyx of Held synapse (refs. 11 and 33 and Fig. 4) supports the notion that L-type Ca^{2+} channels used by ribbon synapses mainly depend on RBPs for localization whereas N- and P/Q-type Ca^{2+} channels found in standard synapses, such as the calyx of Held, depend on both RBPs and RIMs. As a result, the molecular

architecture of nano- and microdomains of Ca^{2+} influx in synapses differs dramatically between ribbon synapses and standard chemical synapses for reasons that remain to be explored but are likely related to the very different functional requirement imposed on these synapses.

Materials and Methods

Mice. In this study, we used constitutive RBP-1 KO, RBP-2 KO, and RBP1,2 double KO (DKO) mice. These mouse lines were generated by crossing RBP-1^{fl}, RBP-2^{fl}, and RBP$1,2^{fl}$ mice to CMV-cre mice that deleted floxed exons in the germline (11) (Fig. 1*A*, *Right*). All experiments involving mice were performed in accordance with Stanford and Federal Guidelines and were approved by the Stanford Institutional Animal Care and Use Committee.

Electrophysiology of Ribbon Synapses. Retinas from light-adapted, 4- to 8-week-old mice were harvested and cut in 200-μm slices using a vibratome. Patch-clamp recordings were performed in whole-cell voltage-clamp configuration either from presynaptic RBC cells (Fig. 4), postsynaptic AII cells (Fig. 8), or both cell types simultaneously (Figs. 2, 3, and 7). Recordings from identified presynaptic RBC cells were used to monitor L-type calcium current density and properties as previously described (31). Quantal release was monitored as postsynaptic mEPSCs using standard approaches (11, 31). Evoked release from ribbon synapses formed between RBC→AII cells was assessed using paired recordings as described previously (31). For details, see *SI Materials and Methods*.

Light Microscopy. We studied the overall structure of the retina by immunohistochemistry, using retina cryosections and antibodies against vGlut1 and PKCα, and confocal microscopy. For details, see *SI Materials and Methods*.

Immunoblotting. Immunoblotting experiments were performed as described elsewhere (33, 39). For details, see *SI Materials and Methods*. A list of antibodies used in the current study with corresponding dilutions and origin are presented in Table S1.

Electron Microscopy. RBP1,2 WT or DKO mice were perfused through the heart with 2% glutaraldehyde/0.5% paraformaldehyde and 0.1 M Na-cacodylate (pH 7.4). The retinas were isolated and stained with 0.5% OsO_4/0.8% K-ferricyanide and then embedded in resins, cut with an ultramicrotome, poststained with uranyl acetate and lead citrate, and analyzed under the electron microscope. For details, see *SI Materials and Methods*.

Data Analysis and Statistics. All quantitative analysis was performed using custom-written macros in IgorPro. Data shown are means ± SEM; statistical analyses used are noted in all figure legends.

ACKNOWLEDGMENTS. We thank Prof. Frank Schmitz (University of Saarland) for the generous gift of Cav1.4 antibodies; and members of the T.C.S. laboratory for invaluable discussions and critical comments on earlier versions of this manuscript.

1. Rosenmund C, Rettig J, Brose N (2003) Molecular mechanisms of active zone function. *Curr Opin Neurobiol* 13:509–519.
2. Schoch S, Gundelfinger ED (2006) Molecular organization of the presynaptic active zone. *Cell Tissue Res* 326:379–391.
3. Südhof TC (2012) The presynaptic active zone. *Neuron* 75:11–25.
4. Han Y, Kaeser PS, Südhof TC, Schneggenburger R (2011) RIM determines Ca^2+ channel density and vesicle docking at the presynaptic active zone. *Neuron* 69:304–316.
5. Kaeser PS, et al. (2011) RIM proteins tether Ca2+ channels to presynaptic active zones via a direct PDZ-domain interaction. *Cell* 144:282–295.
6. Mittelstaedt T, Schoch S (2007) Structure and evolution of RIM-BP genes: Identification of a novel family member. *Gene* 403:70–79.
7. Wang Y, Liu X, Biederer T, Südhof TC (2002) A family of RIM-binding proteins regulated by alternative splicing: Implications for the genesis of synaptic active zones. *Proc Natl Acad Sci USA* 99:14464–14469.
8. Wang Y, Sugita S, Sudhof TC (2000) The RIM/NIM family of neuronal C2 domain proteins. Interactions with Rab3 and a new class of Src homology 3 domain proteins. *J Biol Chem* 275:20033–20044.
9. Hibino H, et al. (2002) RIM binding proteins (RBPs) couple Rab3-interacting molecules (RIMs) to voltage-gated Ca(2+) channels. *Neuron* 34:411–423.
10. Müller M, Genç Ö, Davis GW (2015) RIM-binding protein links synaptic homeostasis to the stabilization and replenishment of high release probability vesicles. *Neuron* 85: 1056–1069.
11. Acuna C, Liu X, Gonzalez A, Südhof TC (2015) RIM-BPs mediate tight coupling of action potentials to Ca(2+)-triggered neurotransmitter release. *Neuron* 87: 1234–1247.
12. Grauel MK, et al. (2016) RIM-binding protein 2 regulates release probability by fine-tuning calcium channel localization at murine hippocampal synapses. *Proc Natl Acad Sci USA* 113:11615–11620.
13. Liu KS, et al. (2011) RIM-binding protein, a central part of the active zone, is essential for neurotransmitter release. *Science* 334:1565–1569.
14. Jarsky T, Tian M, Singer JH (2010) Nanodomain control of exocytosis is responsible for the signaling capability of a retinal ribbon synapse. *J Neurosci* 30:11885–11895.
15. Matthews G, Fuchs P (2010) The diverse roles of ribbon synapses in sensory neurotransmission. *Nat Rev Neurosci* 11:812–822.
16. Schmitz F (2014) Presynaptic [Ca(2+)] and GCAPs: Aspects on the structure and function of photoreceptor ribbon synapses. *Front Mol Neurosci* 7:3.
17. Zanazzi G, Matthews G (2009) The molecular architecture of ribbon presynaptic terminals. *Mol Neurobiol* 39:130–148.
18. Mennerick S, Matthews G (1996) Ultrafast exocytosis elicited by calcium current in synaptic terminals of retinal bipolar neurons. *Neuron* 17:1241–1249.
19. Schwenk F, Baron U, Rajewsky K (1995) A cre-transgenic mouse strain for the ubiquitous deletion of loxP-flanked gene segments including deletion in germ cells. *Nucleic Acids Res* 23:5080–5081.
20. Euler T, Masland RH (2000) Light-evoked responses of bipolar cells in a mammalian retina. *J Neurophysiol* 83:1817–1829.
21. Oesch NW, Diamond JS (2011) Ribbon synapses compute temporal contrast and encode luminance in retinal rod bipolar cells. *Nat Neurosci* 14:1555–1561.
22. Singer JH, Diamond JS (2003) Sustained Ca2+ entry elicits transient postsynaptic currents at a retinal ribbon synapse. *J Neurosci* 23:10923–10933.
23. Protti DA, Llano I (1998) Calcium currents and calcium signaling in rod bipolar cells of rat retinal slices. *J Neurosci* 18:3715–3724.
24. Hoppa MB, Lana B, Margas W, Dolphin AC, Ryan TA (2012) α2δ expression sets presynaptic calcium channel abundance and release probability. *Nature* 486:122–125.
25. Liu C, et al. (2014) The active zone protein family ELKS supports Ca2+ influx at nerve terminals of inhibitory hippocampal neurons. *J Neurosci* 34:12289–12303.
26. Bucurenciu I, Kulik A, Schwaller B, Frotscher M, Jonas P (2008) Nanodomain coupling between Ca2+ channels and Ca2+ sensors promotes fast and efficient transmitter release at a cortical GABAergic synapse. *Neuron* 57:536–545.
27. Eggermann E, Bucurenciu I, Goswami SP, Jonas P (2011) Nanodomain coupling between Ca^{2+} channels and sensors of exocytosis at fast mammalian synapses. *Nat Rev Neurosci* 13:7–21.
28. Fedchyshyn MJ, Wang LY (2005) Developmental transformation of the release modality at the calyx of Held synapse. *J Neurosci* 25:4131–4140.
29. Vyleta NP, Jonas P (2014) Loose coupling between Ca2+ channels and release sensors at a plastic hippocampal synapse. *Science* 343:665–670.
30. Wang LY, Neher E, Taschenberger H (2008) Synaptic vesicles in mature calyx of Held synapses sense higher nanodomain calcium concentrations during action potential-evoked glutamate release. *J Neurosci* 28:14450–14458.
31. Luo F, Bacaj T, Südhof TC (2015) Synaptotagmin-7 is essential for Ca2+-triggered delayed asynchronous release but not for Ca2+-dependent vesicle priming in retinal ribbon synapses. *J Neurosci* 35:11024–11033.
32. Maxeiner S, Luo F, Tan A, Schmitz F, Südhof TC (2016) How to make a synaptic ribbon: RIBEYE deletion abolishes ribbons in retinal synapses and disrupts neurotransmitter release. *EMBO J* 35:1098–1114.
33. Acuna C, Liu X, Südhof TC (2016) How to make an active zone: Unexpected universal functional redundancy between RIMs and RIM-BPs. *Neuron* 91:792–807.
34. Hefft S, Jonas P (2005) Asynchronous GABA release generates long-lasting inhibition at a hippocampal interneuron-principal neuron synapse. *Nat Neurosci* 8:1319–1328.
35. Rozov A, Burnashev N, Sakmann B, Neher E (2001) Transmitter release modulation by intracellular Ca2+ buffers in facilitating and depressing nerve terminals of pyramidal cells in layer 2/3 of the rat neocortex indicates a target cell-specific difference in presynaptic calcium dynamics. *J Physiol* 531:807–826.
36. Ramirez DM, Kavalali ET (2011) Differential regulation of spontaneous and evoked neurotransmitter release at central synapses. *Curr Opin Neurobiol* 21:275–282.
37. Ramirez DM, Khvotchev M, Trauterman B, Kavalali ET (2012) Vti1a identifies a vesicle pool that preferentially recycles at rest and maintains spontaneous neurotransmission. *Neuron* 73:121–134.
38. Sara Y, Virmani T, Deák F, Liu X, Kavalali ET (2005) An isolated pool of vesicles recycles at rest and drives spontaneous neurotransmission. *Neuron* 45:563–573.
39. Grabner CP, et al. (2015) RIM1/2-mediated facilitation of Cav1.4 channel opening is required for Ca2+-stimulated release in mouse rod photoreceptors. *J Neurosci* 35: 13133–13147.
40. Catterall WA (2011) Voltage-gated calcium channels. *Cold Spring Harb Perspect Biol* 3:a003947.
41. Burrone J, Neves G, Gomis A, Cooke A, Lagnado L (2002) Endogenous calcium buffers regulate fast exocytosis in the synaptic terminal of retinal bipolar cells. *Neuron* 33: 101–112.